Precise Tuning of Micelle, Core, and Shell Size by the Composition of Amphiphilic Block Copolymers Derived from ROMP Investigated by DLS and SAXS

Kurt Stubenrauch,[†] Christian Moitzi,[‡] Gerhard Fritz,[‡] Otto Glatter,[‡] Gregor Trimmel,*[,†] and Franz Stelzer[†]

Institute for Chemistry and Technology of Organic Materials, Graz University of Technology, Stremayrgasse 16, 8010 Graz, Austria, and Institute of Chemistry, University of Graz, Heinrichstrasse 28, 8010 Graz, Austria

Received March 1, 2006; Revised Manuscript Received June 8, 2006

ABSTRACT: Self-assembly of well-defined block copolymers in solution has gained attention not only for its scientific value but also for its potential application in nanotechnology. In this study, we present a comprehensive series of synthesized block copolymers that allows conclusions to be drawn how to design micelles by ROMP with defined core−shell geometry and controlled size. We used a general route for the preparation of well-defined block copolymers by ring opening metathesis polymerization (ROMP) with "Grubbs first generation catalyst" $RuCl_2(PCy_3)_2(CHPh)$ (Cy = cyclohexyl). In a first step, we sequentially polymerized *endo,exo*[2.2.1]-bicyclo-2-ene-5,6-dicarboxylic acid dimethylester with *endo,exo*[2.2.1]bicyclo-2-ene-5,6-dicarboxylic acid di-*tert*-butyl ester, to obtain a high control of polymerization and complete characterization of the block copolymers. The polymers were characterized by ^{1}H- and ^{13}C NMR spectroscopy, FT-IR spectroscopy, by GPC, and by DSC. By cleavage of the *tert*-butyl group, the polymer was transformed into an amphiphilic block copolymer. In two series of polymers, we investigated the micelle formation in ethanol by dynamic light scattering (DLS) and small-angle X-ray scattering (SAXS). In the first series, the influence of the block ratio on the size of the micelle, the aggregation number, and the core−shell dimensions were investigated while the overall polymer length was kept constant. In the second series, the block ratio was fixed to 1:1 and the overall polymer length was varied, leading to direct proportionality of the micelle size to the polymer length, while the core-to-shell ratio was constant.

Introduction

The design of highly ordered and nanostructured materials is one of the most challenging tasks in material chemistry. In this context amphiphilic block copolymers with two covalently bonded incompatible blocks are of special interest because of their ability to self-assemble on the nanoscale.[1−3] When a block copolymer is dissolved in a selective solvent, that is a thermodynamically good solvent for one block but a poor solvent for the other block, it associates to form micelles.[4,5] The formation of micelles lends itself to miscellaneous possible applications such as in paints,[6] cosmetics,[7] drug delivery,[8,9] electrical and electrooptical materials,[10−12] metal nanoclusters,[13] biosensors,[14] and gene therapy.[15]

Ring opening metathesis polymerization (ROMP) is a powerful polymerization method of synthesizing block copolymers. The development of well-defined initiator systems during the last 20 years, based on the fundamental work of Grubbs[16,17] and Schrock,[18,19] who were awarded the Nobel Prize in 2005,[20] opened the way for the preparation of well-defined block copolymers with narrow distribution of molecular weights. The tolerance of the ruthenium initiators vs different functionalities and polarities exceeds that of most other polymerization techniques and the living nature of ROMP[16] makes it particularly valuable for the preparation of block copolymers with different functionalities and low polydispersity as already demonstrated by several groups.[21,22] Furthermore, the possibility of side- and end-functionalization of these polymers opens way to new highly ordered smart materials. It has been shown that defined amphiphilic block copolymers can be obtained by ROMP. Several aspects were investigated, such as the formation of stable micelles and nanoparticles,[23−27] the use as drug delivering material,[28,29] as polymers with special electrooptical and electroactive properties[30−33] and for the preparation of inorganic nanoparticles.[34−36] For most of the above-mentioned applications, the self-assembly at the nanoscale has to be very precise and homogeneous. This can only be achieved by a very well controlled synthesis of the block copolymers. To our knowledge, no comprehensive study on the micelle formation behavior of a complete series of block copolymers derived from ROMP exists in the literature and because of the increasing importance of such polymers a detailed study is overdue.

Herein we show that the micelle size as well as the core−shell dimensions of amphiphilic block copolymers in solution can be perfectly tuned through the block copolymer composition of polymers prepared via ROMP. As the lyophobic block we chose *endo,exo*[2.2.1]bicyclo-2-ene-5,6-dicarboxylic acid dimethylester (monomer **A**) as it is a very easily accessible monomer and esters are also convenient for ring opening metathesis polymerization.[37−39] *endo,exo*[2.2.1]Bicyclo-2-ene-5,6-dicarboxylic acid was selected as the lyophilic part since the acid functionality is a representative unit for lyophilic blocks. The "first generation Grubbs" initiator $RuCl_2(PCy_3)_2(CHPh)$ (Cy = cyclohexyl) was used as the catalyst. With this catalyst a low polydispersity polymer of acid functionalized monomers

* Corresponding author: E-mail: gregor.trimmel@tugraz.at. Telephone: ++43316-8734958. Fax: ++43316-8738951.
† Institute for Chemistry and Technology of Organic Materials, Graz University of Technology.
‡ Institute of Chemistry, University of Graz.

10.1021/ma060451p CCC: $33.50
Published on Web 07/27/2006

Table 1. Characteristics of the Amphiphilic Block Copolymers

	sample no.	m^a	n^b	$X_m{}^c$	X_m NMR^d	M_{calcd},^{e} g/mol	M_n(GPC),^{f} g/mol	M_n(NMR),^{g} g/mol	PDI^h	T_g,^{i} °C
series A	1	200	0			41 637	47 100		1.13	82.4
	2	175	25	7	7.2	44 317	44 900		1.15	82.5
	3	150	50	3	3.2	46 408	49 300		1.15	80.3
	4	125	75	1.6	1.7	48 562	53 600		1.14	83.2
	5	100	100	1	1.0	49 737	54 100		1.13	83.4
	6	75	125	0.6	0.62	52 699	51 200		1.11	83.8
	7	50	150	0.3	0.31	54 774	54 900		1.07	83.7
	8	25	175	0.14	0.14	56 878	54 000		1.07	83.5
	9	0	200			58 982	54 700		1.05	83.4
series B	5	100	100	1	1.0	49 737	54 100		1.13	83.4
	10	75	75	1	0.90	37 544	35 900		1.16	81.9
	11	40	40	1	1.0	20 384	24 900	20 400	1.08	n.d.
	12	30	30	1	1.1	15 194	18 300	15 700	1.10	n.d.
	13	20	20	1	1.2	10 194	13 200	11 150	1.07	77.0

[a] Theoretical number of lyophobic units (monomer **A**). [b] Theoretical number of lyophilic units (monomer **B**). [c] Theoretical ratio of lyophobic block/lyophilic block. [d] Ratio of lyophobic block/lyophilic block determined via integration of the ^{1}H NMR spectra (relaxation time 10 s). [e] Calculated molecular weight. [f] Number average of the molecular weight distribution determined by GPC. [g] Number average of the molecular weight distribution determined by NMR spectroscopy (end group analysis). [h] Polydispersity index determined by GPC. [i] Glass transition temperature determined by differential scanning calorimetry.

could not be obtained by direct polymerization and small amounts of unpolymerized monomer were found even after long reaction times.

Several research groups reported the synthesis of polymers containing *endo,exo*[2.2.1]bicyclo-2-ene-5,6-dicarboxylic acid units, protected with trimethylsilyl groups. Since this protection group is easily hydrolyzed, GPC measurements have either not been performed or only with difficulties.[23,25,34,40,41] For the production of well-defined low polydispersity block copolymers the evaluation of the PDI is necessary. Another approach proposed by Grubbs et al.[42] and Buchmeiser et al.[43] was the polymerization of *endo,endo*[2.2.1]bicyclohept-2-ene-5,6-dicarboxylic anhydride and subsequent hydrolysis. However as a result of the low solubility of the obtained polymers, chains of only 15 monomer units could be isolated.

We introduced *tert*-butyl ester as a protection group for the acid functionalities to guarantee a reproducible synthesis and characterization of the block copolymers. After full characterization of the polymers by NMR and IR-spectroscopy, GPC, and DSC, trifluoroacetic acid was used to remove the *tert*-butyl protection group, leading to amphiphilic block copolymers. We synthesized two series of block copolymers, one with altered conformation and the other with altered length (Table 1). For the first series the overall monomer/catalyst ratio was kept the same (200:1) but the ratio of lyophilic monomer to lyophobic monomer was altered. For the second series the lyophilic-to-lyophobic ratio was kept the same, namely 1:1, but the overall monomer/catalyst ratio was varied. Solutions of these block copolymers in ethanol were investigated by dynamic light scattering (DLS) to determine the hydrodynamic radius of the formed micelles. Small-angle X-ray scattering (SAXS) was used to determine the aggregation number, shape and the core and shell size of the micelles. SAXS in particular is a very powerful tool to get detailed integral information about the internal structure of aggregates. We herein describe the first systematic study of micelle behavior of series of amphiphilic block copolymers derived from ROMP.

Experimental Section and Theory

All chemicals were purchased from commercial sources and used without further purification. CH_2Cl_2 was distilled over CaH_2 and degassed with argon. *endo,exo*[2.2.1]Bicyclo-2-ene-5,6-dicarboxylic acid dimethylester, monomer **A**, was kindly supplied by Orgentis Chemicals; *endo,exo*[2.2.1]bicyclo-2-ene-5,6-dicarboxylic acid was prepared according to literature.[44] All experiments were carried out under inert atmosphere in a glovebox.

GPC. The weight and number-average molecular weights (M_w and M_n) as well as the polydispersity index (PDI) were determined by gel permeation chromatography with THF as solvent using the following arrangement: Merck Hitachi L6000 pump, separation columns of Polymer Standards Service, 8 × 300 mm STV 5 μm grade size (10^6, 10^4, and 10^3 Å), and a combined refractive index−viscosity detector from Viscotec, Viscotec 200. Polystyrene standards purchased from Polymer Standard Service were used for calibration.

^{1}H NMR and ^{13}C NMR spectra were recorded on a Varian INOVA 500 MHz spectrometer operating at 499.803 MHz and 125 687 MHz, respectively, and were referenced to $SiMe_4$. A relaxation delay of 10 s and 45° pulse were used for acquisition of the ^{1}H NMR spectra to guarantee accurate integration of the corresponding signals.

Differential scanning calorimetry (DSC) measurements were carried out on a Perkin-Elmer Pyris Diamond under a nitrogen flow of 20 mL/min and a heating rate of 10 °C/min. Glass transition temperatures (T_g) from the second heating run were read as the midpoint of change in heat capacity.

FT-IR spectra were recorded with a Perkin-Elmer Spectrum One instrument (spectral range between 4000 and 450 cm^{-1}). All FT-IR spectra of the samples were recorded in transmission mode (films on CaF_2 disks).

For the DLS measurements we used a laboratory built goniometer, which was equipped with single mode fiber optics and an ALV single photon detector. The light source was a Verdi V5 diode laser from Coherent with a wavelength of 532 nm and a maximum output power of 5 W (typically laser power used 0.5 W). The data acquisition was performed with an ALV 5000 multiple τ digital correlator. This allows a minimum time interval of 12.5 ns for the correlation function. The ALV-5000/E software package was used to record and store the correlation functions. All experiments were carried out at 25 °C and at a scattering angle of 90°. Each sample was measured 10 times for 60 s. The obtained correlation functions were averaged and used for calculation of the size distributions. We used the ORT[45] software to determine the intensity weighted size distribution functions.

The SAXS equipment was a SAXSess camera (Anton-Paar, Graz, Austria) using an X-ray generator (Philips, PW 1730/10) operated at 40 kV and 50 mA with a sealed-tube Cu anode. A Göbel mirror was used to convert the divergent polychromatic X-ray beam into a collimated line-shaped beam of Cu Kα radiation ($\lambda = 0.154$ nm). The 2D scattering pattern was recorded by an imaging-plate detector (model Fuji BAS1800 from Raytest, Straubenhardt, Germany) and integrated into the one-dimensional scattering function $I(q)$ using

SAXSQuant software (Anton-Paar). The samples were filled at room temperature into the sample holder (quartz capillary in a metal block, temperature controlled by a Peltier element, ±0.1 K) and measured at 25 °C.

Synthesis. *endo,exo*[2.2.1]Bicyclo-2-ene-5,6-dicarboxylic Acid Di-*tert*-butyl Ester (Monomer B), Modified Literature Synthesis.[46] Under inert atmosphere *tert*-butyl alcohol (7.3 g, 98.1 mmol) and pyridine (10.8 g, 136.9 mmol) were dissolved in dry CH_2Cl_2. Under ice cooling *endo,exo*[2.2.1]bicyclo-2-ene-5,6-dicarboxylic acid chloride (10.0 g, 45.6 mmol) was dropped into the reaction mixture and stirred overnight at room temperature. The reaction mixture was filtered to remove the pyridine salt and extracted with dichloromethane. The organic layer was extracted with 5% hydrochloric acid solution and saturated sodium bicarbonate and dried with sodium sulfate. Column chromatography with cyclohexane/ethyl acetate (10:1) as the solvent was used to purify the product (yield 75%).

^{1}H NMR (δ, 20 °C, $CDCl_3$, 500 MHz): 6.26 (dd, 1H, CH^6), 6.05 (dd, 1H, CH^5), 3.23 (t, $^3J_{HH}$ = 4,1 Hz, 1H, CH^3), 3.17 (s, 1H, CH^4), 3.04 (s, 1H, CH^1), 2.53 (dd, 1H, CH^2), 1.57 (d, $^3J_{HH}$ = 8,7 Hz, 1H, CH^{7a}), 1.45 (s, 9H, CH_3), 1.41 (s, 10H, (CH_3),(CH^{7b}). ^{13}C-{^{1}H} NMR (δ, 20 °C, $CDCl_3$, 125 MHz): 173.9, 172.7 (C═O), 137.5, 134.8 (C^5, C^6), 80.4, 80.2 (−$C(CH_3)_3$), 48.7, 48.1, 47.8, 47.2, 45.8 (C^3, C^1, C^7, C^2, C^4), 28.1 (−CH_3). FT-IR (films on CaF_2, cm^{-1}): 3066 (w, $\nu_{H-C=C}$), 2978 (s), 2934 (m), 2876 (m), 1724 (s, $\nu_{C=O}$), 1572 (w, $\nu_{C=C}$),1367 (s), 1152 (s), 848 (m), 719, 694 (w, $\nu_{H-C=C\ def}$).

General Polymerization Procedure. As example for polymer **5**: The polymerization was carried out in a glovebox. Monomer **A** (120.0 mg, 0.57 mmol) and initiator $RuCl_2(PCy_3)_2$(CHPh) (4.7 mg, 0.006 mmol) were dissolved in 2 mL of dichloromethane each and the monomer was added to the catalyst solution. The reaction mixture was stirred for 24 h and the absence of monomer **A** was confirmed by TLC. Monomer **B** (168.0 mg, 0.57 mmol) was dissolved in 2 mL of dichloromethane and added to the reaction mixture. It was stirred for another 24 h. The polymerization was stopped with 5 drops of cold ethyl vinyl ether and the reaction stirred for further 30 min. The solvent was then reduced to half the volume and the polymer was precipitated in cold methanol. The methanol was decanted off and the product was dried in a vacuum oven overnight at 40 °C (yield 98%).

^{1}H NMR of **5** protected (δ, 20 °C, $CDCl_3$, 500 MHz): 5.57−5.12 (m, 2H, ═CH), 3.66, 3.62 (vd, 3H, OCH_3), 3.36−2.51 (m, 4H, $CH^{1,2,3,5}$), 1.92 (bs, 1H, CH^4), 1.58−1.34 (bs, 10H, CH,^{4} OC-$(CH_3)_3$). ^{13}C{^{1}H} NMR of **5** protected (δ, 20 °C, $CDCl_3$, 125 MHz): 175.3−172.4 (*C*═O), 134.8−129.8 (═*C*H), 80.8 (*C*$(CH_3)_3$), 54.8−29.7 (O−*C*H_3, *C*H, *C*H_2), 28.5 C(*C*$H_3)_3$). FT-IR (films on CaF_2, cm^{-1}): 2977(s), 2953 (s), 1728 (s, $\nu_{C=O}$), 1367 (s), 1151 (s), 972, (w, $\nu_{trans\ C=C}$), 736 (w, $\nu_{cis\ C=C}$).

After characterization the product was dissolved in 8 mL of dichloromethane and 4 mL of trifluoroacetic acid was added to remove the protecting group. The reaction mixture was allowed to stir overnight at ambient temperature and was then poured into toluene. The solvents were removed under reduced pressure and the solid was dissolved in THF and precipitated in cold pentane. The product was collected and dried overnight under vacuum at 40 °C (yield 98%).

^{1}H NMR of **5** deprotected (δ, 20 °C, DMSO-d_6, 500 MHz): 12.82−11.66 (bs, 0.5H, COOH), 5.61−5.09 (m, 2H, ═CH), 3.61, 3.58 (vd, 2.7H, OCH_3), 3.38−2.55 (m, 4H, $CH^{1,2,3,5}$), 1.99 (bs, 1H, CH^4), 1.40 (bs, 1H, CH^4). ^{13}C{^{1}H} NMR of **5** deprotected (δ, 20 °C, $CDCl_3$, 125 MHz): 175.9−173.3 (*C*═O), 134.3−130.2 (═*C*H), 80.8 (*C*$(CH_3)_3$), 54.1−30.0 (O−*C*H_3, *C*H, *C*H_2). FT-IR (films on CaF_2, cm^{-1}): 3620−2260(b, COOH), 2977(s), 2953 (s), 1728 (s, $\nu_{C=O}$, COOMe), 1706 ($\nu_{C=O}$, COOH), 1367 (s), 1151 (s), 972, (w, $\nu_{trans\ C=C}$), 736 (w, $\nu_{cis\ C=C}$).

Determination of the Size of the Micelles by DLS. Dynamic light scattering (DLS) is a widely used method for the determination of sizes and dynamics in colloidal systems. It measures the time-dependent fluctuations of the intensity of the scattered light at a fixed scattering angle. From the fluctuation rate information about diffusion constants can be gained. By assuming diffusion of noninteracting spherical particles the particle size can be calculated thereof via the Stokes−Einstein relation. The details about the data evaluation are not given here as they can be found in several textbooks.[47−50] It has to be noted that the finite concentration of the micelles has some influence on the diffusion and causes therefore a certain error. It was not possible to account for this by performing DLS measurements as a function of dilution because of the self-assembled nature of the micelles. However, the magnitude of the error made can be estimated by

$$D_C = D_0(1 + 1.56\phi) \tag{1}$$

where D_0 is the free particle translational diffusion constant, ϕ is the volume fraction and D_C is the measured diffusion coefficient. The volume fraction can be obtained from the SAXS experiments. A discussion of the effect of finite concentration is given in the Results and Discussion.

Determination of the Aggregation Number by Small-Angle X-ray Scattering. The aggregation number of micelles can be determined from small-angle X-ray scattering (SAXS) data, as the forward scattering intensity at zero scattering angle depends linearly on the molecular or aggregate weight of the scattering particles. To determine the forward scattering intensity it is necessary to put the measured scattering curve on absolute scale. This was done by measuring the scattering intensity of water, which only depends on the physical properties of isothermal compressibility and on the electron density. The scattering intensity $I(0)$ of water at 25 °C is 0.01633 (cm^{-1}).[54] By multiplying all scattering functions with an experimental factor, it is possible to place them on absolute scale. The detailed procedure was described by D. Orthaber et al.[55]

As we used slit collimation of the primary beam in our experimental setup to increase the flux and to improve the signal quality, desmearing of the scattering curve was required. This was done automatically by our indirect Fourier transformation (IFT) algorithm.[56−58] Once the desmeared scattering curve on absolute scale is known, one can determine the forward intensity at zero scattering angle by Fourier extrapolation. To do this extrapolation correctly, it is important to take interparticle interactions into account, even if the concentration of the polymer was only 1 wt %. In this study interactions were modeled using a hard sphere structure factor.[59] However, as the micelles are not real hard spheres, the model's result has to be viewed as an effective structure factor. This means that the model parameters have to be interpreted as the effective volume fraction and the effective radius. In any case the effective structure factor is fitted to describe the same decrease in forward scattering. And that is the essential requirement to determine the aggregation number. The structure factor was determined for the polymer with smallest molecular weight with our GIFT[59−61] routine (micellar radius about 8 nm). As all solutions have the same concentration the obtained volume fraction was used for all samples. The volume fraction was not determined for all samples independently because for the polymers with higher molecular weight the size of the micelles reaches the resolution limit of our instrument (about 40 nm). Therefore, the determination of the structure factor becomes less precise with the increasing size of the micelles. The molecular weight of the scattering micelle can be calculated according to eq 2.[62]

$$M = \frac{d\Sigma\,(0)}{d\Omega}(N_A/c\Delta\rho_M{}^2) \tag{2}$$

M is the molecular weight, $d\Sigma(0)/d\Omega$ (cm^{-1}) is the forward scattering intensity at $q = 0$, c (g/cm^3) is the polymer concentration, N_A is the Avogadro number, and $\Delta\rho_M$ (cm/g) is the scattering length difference per mass:

$$\Delta\rho_M = \Delta\rho\bar{\nu} \tag{3}$$

The scattering length difference $\Delta\rho$ (cm^{-2}) can be calculated with the known chemical composition of the polymer and the solvent.

Scheme 1. Synthesis of Block Copolymers with ROMP

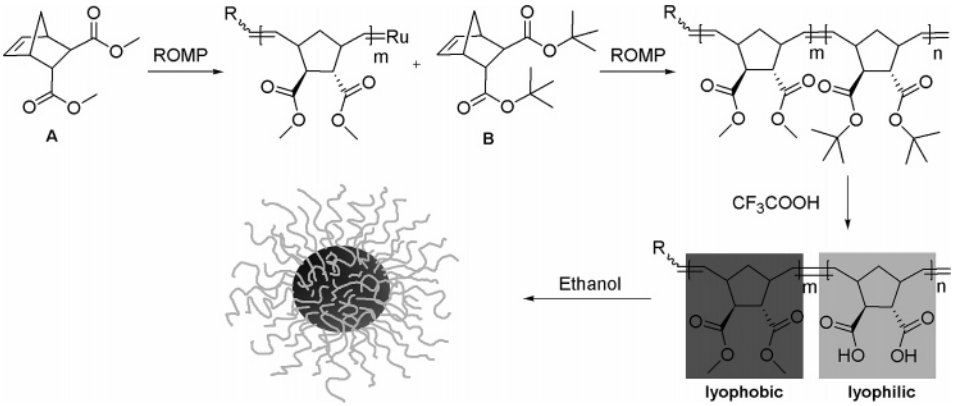

$\bar{\nu}$ (cm^3/g) is the specific volume of the polymer in solution, which can be calculated via density measurement of the solvent and the solution (DMA 5000; Anton Paar, Graz, Austria).

If one knows the molecular weight of a single polymer molecule, the aggregation number can easily be calculated by the aggregate molecular weight of the micelle determined with eq 2. Considering the standard uncertainties of the used values for the molecular weight determination, especially those of $d\Sigma(0)/d\Omega$ and $\Delta\rho_M$, we can estimate the uncertainty of the resulting molecular weights of the aggregates as about 10%.[55]

Indirect Fourier Transformation and Convolution Square Root. The methodology for analyzing small-angle scattering data using indirect Fourier transformation[56−58] followed by deconvolution[63−65] has been described in detail elsewhere. The discussion here will describe only the main ideas. Using this approach, information about the shape, size, and internal structure of the micelles can be gained.

For a particle of an arbitrary shape with a scattering density difference of $\Delta\rho(r)$, the pair distance distribution function $p(r)$ (PDDF) is given by

$$p(r) = r^2\Delta\tilde{\rho}^2(r) \tag{4}$$

where $\Delta\tilde{\rho}^2(r)$ is the convolution square of $\Delta\rho(r)$ averaged for all directions in space. This averaging causes no loss of information in the case of particles with special symmetry.

The PDDF is related to the scattered intensity $I(q)$ by a Fourier transformation and enables the determination of the overall shape and size of the scattering objects.

$$I(q) = 4\pi\int_0^\infty p(r)\frac{\sin(qr)}{qr}\mathrm{d}r \tag{5}$$

where q is the magnitude of the scattering vector q, defined as

$$q = \frac{4\pi}{\lambda}\sin\left(\frac{\theta}{2}\right) \tag{6}$$

where λ is the wavelength of the incident radiation and θ is the angle between the scattered and incident beam. In the case of spherical geometry, the deconvolution of the PDDF gives the radial contrast profile $\Delta\rho(r)$ in electron density, which gives information about the internal structure of the scattering particles. Most spherical micelles have a core−shell type structure, with a lyophobic core and a lyophilic shell also containing bound solvent molecules. As long there is a difference in electron density, the radius of the core and the thickness of the shell can be seen directly from the radial contrast profile $\Delta\rho(r)$.

Determination of the End-to-End Distance of the Polymer. To estimate the size of polymer coils, the persistence length of polymer **9** consisting only of lyophilic monomers was determined. By Guinier extrapolation of the desmeared scattering curve toward q equal zero the radius of gyration R_g was measured. For a self-avoiding walk model for the description of the coil structure, the radius of gyration depends on the number of monomers N in the following way

$$R_g = cN^{0.588} \tag{7}$$

where c is a constant, which can be determined from the measurement of the radius of gyration of a completely lyophilic polymer. By applying eq 7 the radii of gyration for the lyophilic parts of all used polymers can be calculated. The end-to-end distance can be obtained by applying

$$R_E \approx \sqrt{6}R_g \tag{8}$$

Results and Discussion

The introduction of the *tert*-butyl group as protection group for the acid functionality solves the problem of incomplete characterization as well as the problem of insufficient control over the polymerization parameters of the lyophilic block. The *tert*-butyl derivative (monomer **B**) is easily accessible by a simple esterification reaction of the carboxylic acid chloride and *tert*-butyl alcohol.[46] Using "Grubbs first generation" catalyst, we obtained full conversion of monomer **B** as well as of monomer **A** within 24 h leading to well-defined homopolymers. For the study of micelle formation we prepared two series of block copolymers consisting of monomer **A** as a lyophobic block and monomer **B**—as a disguised lyophilic block (Scheme 1). For the first series the overall polymer length was kept the same but the ratio of lyophilic monomer to lyophobic monomer was altered (**1**−**9**). For the second series the lyophilic-to-lyophobic ratio was fixed to 1:1, but the overall polymer length was varied (**5**, **10**−**13**). The block sizes and the block ratios of the different polymers are shown in Table 1.

The molecular weight distribution and the polydispersity index were determined using GPC. The physico-chemial data of the investigated block copolymers are listed in Table 1. The GPC measurements were calibrated against polystyrene standards; nevertheless, the calculated and determined masses are in good agreement. All GPC chromatograms obtained show a monomodal distribution confirming a defined growth of the second block, as depicted in Figure 1. The polydispersity indices are low and in the range from 1.05 to 1.15. In series A, all block copolymers have about the same molecular weight with a small increase from **1** to **9** with increasing content of monomer **B**, whereas in series B the expected decrease of the molecular weight is observed. By end group analysis of the ^{1}H NMR spectra, it was possible to obtain the absolute number-average of the molecular weight distribution of the three low-molecular polymers **11**, **12**, and **13**. The obtained values are between the theoretical calculated ones and the ones determined by GPC.

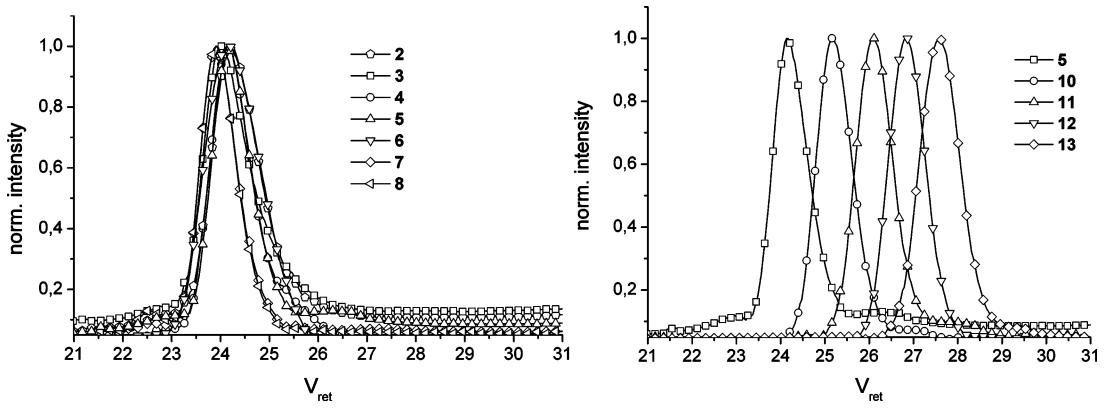

Figure 1. Gel permeation chromatograms for block copolymer series A and B.

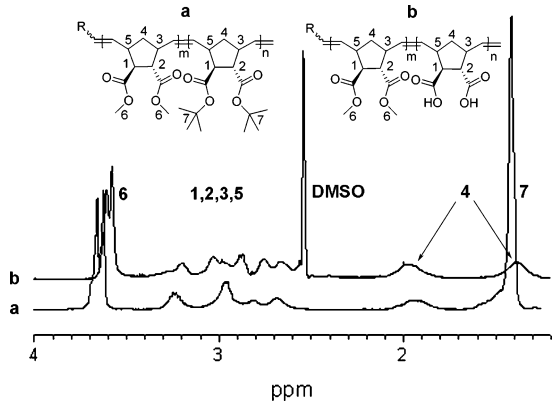

Figure 2. NMR spectra of **5** before and after cleavage of the *tert*-butyl group (spectrum a is performed in $CDCl_3$, spectrum b in DMSO-d_6).

However, end group analysis was not possible for the other polymers; therefore, the GPC data was used for further calculations for these polymers. The obtained GPC and NMR data give proof for the composition and the low polydispersity of the block copolymers.

The glass transition temperatures (T_g) of the homopolymers **1** and **9** are almost identical, therefore we see for all polymers transition temperatures of about 83 °C. The glass transition temperature is observed to be slightly decreasing with the molecular weight from 83 °C for **5** to 77 °C for **13**.

For the transformation into amphiphilic block copolymers, the *tert*-butyl groups are cleaved by treating the polymer with trifluoroacetic acid. This detachment is selective and complete even in the presence of methyl esters as proved by NMR measurements, shown in Figure 2, and FT-IR spectroscopy.

After treatment with trifluoroacetic acid, the *tert*-butyl peak (7) at 1.4 ppm disappears in spectrum b whereas the integral over the methyl peak (6) at 3.6 ppm stays the same. The small, broad remaining peak at 1.4 in spectrum b is assigned to one of the protons at the bridge position in the cyclopentane ring (4). In addition, a broad peak of the acidic protons is visible at around 12 ppm. From the spectra, it can be concluded that the cleavage is complete, and the yield for the deprotection step is practically quantitative. The infrared spectra also confirm this reaction. Before cleavage, a strong vibration band at 1728 cm^{-1} can be observed due to the carbonyl-stretching vibrations of both the esters. After cleavage, this strong peak is weaker, and depending on the block ratio, the vibration of the carboxylic acid at 1706 cm^{-1} appears accompanied by a very broad peak between 3500 and 2500 cm^{-1} due to the acidic OH stretching vibrations of the free carboxylic acid.

GPC measurements of the deprotected amphiphilic block copolymers could not be carried out due to interaction with the used column material. The integration values of the ^1H NMR spectra of the free amphiphilic block copolymer confirmed the intactness of the main chain. However, the integration values found are strongly dependent on the used solvent.[29] The integration data displays correct values only if both blocks are fully dissolved and micelle formation does not occur. In the case of our system the polymers were quite good soluble in DMSO-d_6 with the exception of the most lyophobic polymers **2** and **3**. These two polymers showed values which were too low for the methyl protons which are caged in the core of the micelle. However using $CDCl_3$ as solvent for **2**, the findings of the methyl group are too high. We assume that inverse micelles are formed in this solvent. The effect of micelle formation was also demonstrated by recording ^1H NMR spectra of one polymer (**5**) in two different solvents DMSO-d_6 and CD_3OD. The integration of the methyl peak in DMSO-d_6 is in good agreement with the spectrum of the protected polymer in $CDCl_3$, whereas in CD_3OD the methyl protons of the methoxy groups in the lyophobic block are underrepresented and the signal is very broad. Methanol as well as ethanol are selective solvents for the acid functionalized block and therefore suitable for self-assembly studies in solution. Because of the toxicity of methanol, ethanol was used for the investigations.

DLS. Both block copolymer series were investigated with DLS. To determine the aggregate size in ethanol, solutions containing 1 wt % polymer were used. In Figure 3, the volume weighted size distribution functions $D_v(R)$ of series B, calculated via inverse Laplace transformation from the measured correlation functions, are shown. All the block copolymers **5** and **10**−**13** of series B, varying molecular weight of the polymers and constant lyophobic to lyophilic rate ($X_m = 1{:}1$), show formation of aggregates. The aggregate size decreases with decreasing molecular weight of the polymers, giving hydrodynamic radii from 20 to 8 nm for polymers from 42 kDa to 10 kDa. For all polymers the determined radius is apparently too large to origin from one single polymer molecule, so it is clear that micelles are formed. It is impossible to calculate the aggregation number from the aggregate size determined by DLS because it is not known how much solvent is incorporated into the micelles.

In Figure 4, the results of the DLS measurements of the polymers **4**−**8** of series A are shown. In series A the overall monomer/catalyst ratio was kept constant (similar molecular weight; 35 kDa < M_n < 45 kDa) but the lyophobic-to-lyophilic ratio X_m was varied from 7.3 (very lyophobic) to 0.14 (very

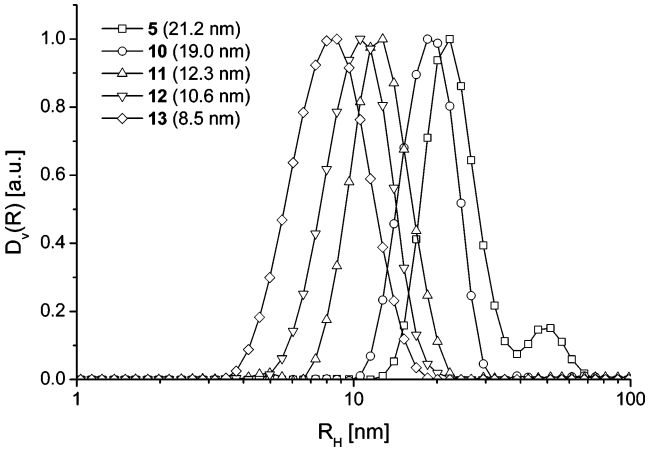

Figure 3. Volume weighted size distribution functions $D_v(R)$ of 1 wt % solutions of polymers **5** and **10**−**13** (series B) having varying molecular weight and constant lyophobic to lyophilic rate ($X_m = 1$) determined with DLS. The molecular weight is decreasing from **5** (42 kDa) to **13** (10 kDa). In brackets the R_H values of the distribution maxima are shown.

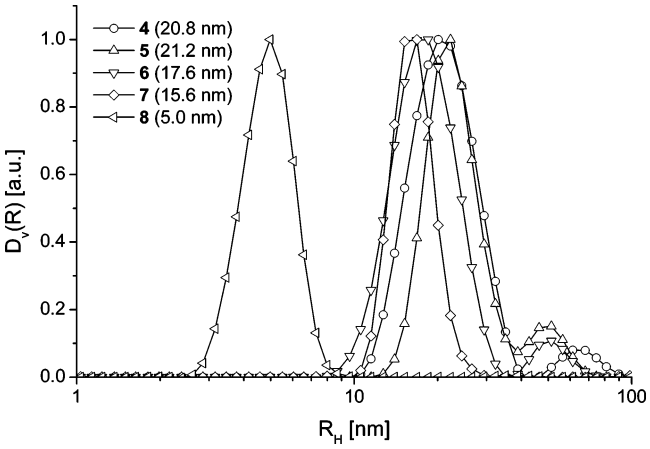

Figure 4. Volume weighted size distribution functions $D_v(R)$ of 1 wt % solutions of polymers **4**−**8** (series A) having constant overall monomer/catalyst ratio (35 kDa < M_n < 45 kDa) and varying lyophobic to lyophilic rate X_m, determined with DLS. The ratio X_m is decreasing from **4** (1.7) to **8** (0.14). In brackets the R_H values of the distribution maxima are shown.

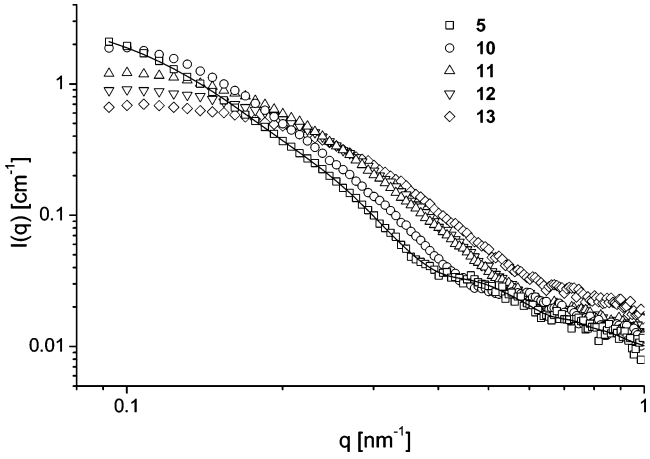

Figure 5. Smeared scattering curves on absolute scale of 1 wt % polymer in ethanol. The molecular weight of the polymers **5**, **10**−**13** of series B is decreasing from **5** (42 kDa) to **13** (10 kDa). The ratio X_m is 1 for all samples of this series. The line is the fit of the IFT calculation. For clarity just one fit is shown, the other fits are of about the same quality.

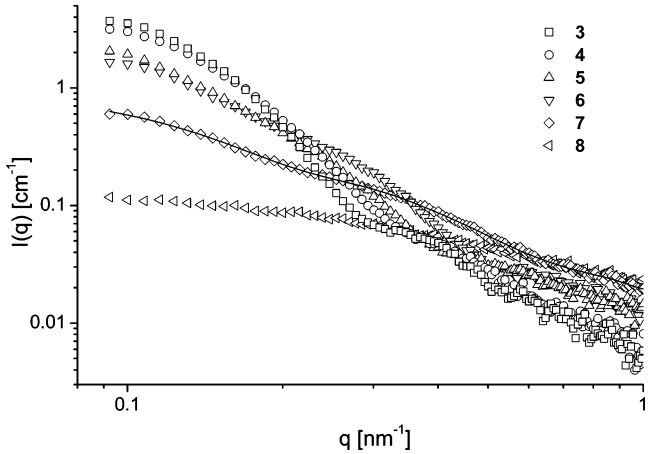

Figure 6. Smeared scattering curves on absolute scale of 1 wt % polymer in ethanol. The molecular weight of polymers **3**−**8** of series A is between 35 and 45 kDa. The ratio X_m is decreasing from **3** (3.2) to **8** (0.14).). The line is the fit of the IFT calculation. For clarity just one fit is shown; the other fits are of about the same quality.

lyophilic). The most lyophobic polymer **2** was not soluble at all, and the solution of the polymer **3** stayed turbid. As a result of multiple scattering no accurate evaluation of the DLS data was possible for this sample. All other solutions were completely transparent. With decreasing X_m the micellar radius decreases slightly from 21 for polymer **4** ($X_m = 1.7$) to 16 nm for polymer **7** ($X_m = 0.31$). Therefore, the composition of block copolymers of about the same chain length does not have a significant impact on the micelle size. The determined particle radius for the most lyophilic polymer **8** is much smaller (5 nm). This gives strong evidence for a solution of single polymer molecules, compared to formed micelles in all other samples of this series.

SAXS. To confirm the data obtained by DLS and to get information about the aggregation number as well as the core and the shell size, SAXS measurements were performed. The smeared scattering curves of the polymer solutions (1 wt %) **5** and **10**−**13** of the series B are shown in Figure 5. One can clearly see that the forward scattering intensity, which depends linearly on the molecular weight of the scattering particles, increases with increasing molecular weight of the single polymer molecules. To extrapolate the forward scattering intensity at $q = 0$ the GIFT routine was applied on the solution of the smallest polymer molecule **13** to determine the form factor $P(q)$ and structure factor $S(q)$ simultaneously. A hard sphere structure factor model was used. The excluded volume effect at the determined volume fraction (1.6%) decreases the forward scattering by about 12%. It is therefore very important to use a structure factor for the determination of the forward scattering even at this relatively low polymer concentration. For the large polymers of this series the determination of the volume fraction was not as accurate as for the smallest polymer because the aggregate size reaches the resolution limit of our instrument. It was assumed that the volume fraction does not change significantly, as in all samples the same polymer concentration was used. This means that the number of micelles decreases if the size of the micelles is increasing. The same value (1.6 vol %) was therefore used for all samples. The volume fraction which was determined from the structure factor model can be used to estimate the error of the DLS experiments made because of finite particle concentration according to eq 1. The resulting deviation of the measured diffusion constant from the theoretical one at infinite dilution is approximately 2.5%.

Table 2. Summary of the Determination of the Molecular Weight of the Aggregates in Solution

	sample no.	I_0,[a] cm^{-1}	ρ_{sample},[b] g/mL	$\rho_{solvent}$,[b] g/mL	$M_{dep,calcd}$,[c] g/mol	X_m[d]	M_{agg},[e] g/mol	N_{agg}[f]
series A	3	195.0	0.792783	0.789455	43 600	3.2	12529300	287
	4	143.0	0.792705	0.789455	44 400	1.7	9713000	219
	5	120.3	0.792866	0.789465	42 100	1.0	7343800	174
	6	75.5	0.792978	0.789455	35 800	0.62	4250600	119
	7	21.2	0.793133	0.789455	37 800	0.31	1079800	29
	8	1.9	0.793184	0.789455	35 400	0.14	94 700	3
series B	5	120.3	0.792866	0.789465	42 100	1.0	7343800	174
	10	75.1	0.793057	0.789465	27 900	0.9	4043500	145
	11	26.8	0.792783	0.789465	15 800	1.0	1735400	110
	12	15.9	0.792617	0.789420	12 300	1.1	1121500	91
	13	10.1	0.792783	0.789465	8900	1.2	652 100	73

[a] Forward scattering intensity. [b] Specific densities of the solutions ρ_{sample} and the solvent $\rho_{solvent}$, variations in the solvent density are because of changing atmospheric pressure. [c] Calculated molecular weight based on GPC data of Table 1, except for polymers **11**, **12**, and **13**, the NMR-spectroscopy data was used. [d] Ratio of lyophobic block/lyophilic block. [e] Aggregate molecular weight, calculated according to eq 7. [f] Aggregation number.

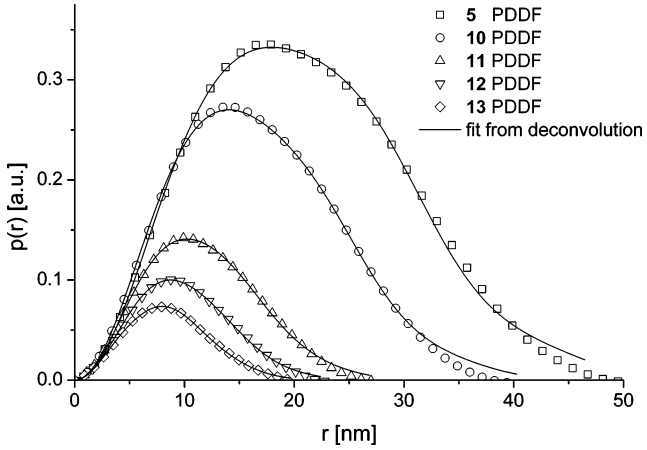

Figure 7. Pair distance distribution functions $p(r)$ (symbols) of polymers **5**, **10**−**13** (series B) having varying molecular weight and constant lyophobic-to-lyophilic ratio ($X_m = 1$, series B) determined via IFT from SAXS curves. The molecular weight is decreasing from **5** (42 kDa) to **13** (10 kDa). The lines are the corresponding fits from the deconvolution.

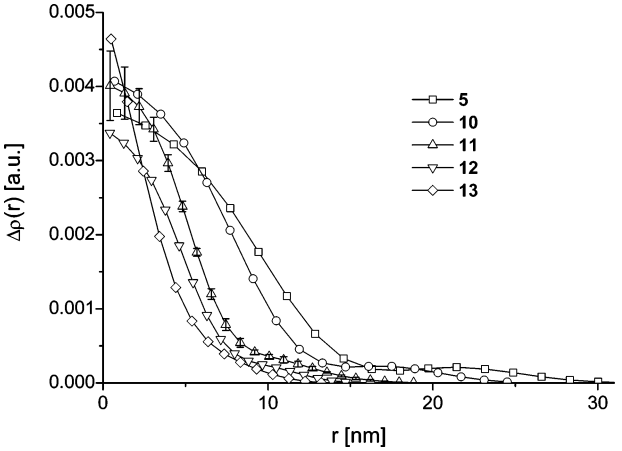

Figure 8. Radial contrast profile $\Delta\rho(r)$ of polymers **5**, **10**−**13** (series B) having varying molecular weight and constant lyophobic-to-lyophilic ratio, determined via deconvolution from the PDDF. The molecular weight is decreasing from **5** (42 kDa) to **13** (10 kDa). For clarity the error bars are only shown for one curve.

The polymers **3**−**8** of series A were measured in the same way. The solution of **3** ($X_m = 3.2$, very turbid) was also investigated, which was not possible with DLS. The corresponding smeared scattering curves are shown in Figure 6. The extrapolated scattering intensities after desmearing and taking a structure factor into account are summarized in Table 2.

For calculation of the aggregation number, we used for polymers **11**, **12**, and **13** the molecular weight values obtained from NMR spectroscopy, whereas for all other polymers we used calculated values based on the GPC data of Table 1. We estimate the deviation from the absolute values of the aggregation numbers to be about 15% for those polymers; however the obtained values in Table 2 demonstrate very well the general trend of both series. In series A the aggregation number decreases with decreasing lyophobic-to-lyophilic ratio X_m dramatically from 287 to 3. The aggregation number 3 of the most lyophilic polymer **8** corresponds practically to monomers as it is known that in surfactant systems even below the cmc oligomers with rather low aggregation numbers are present.[66] In series B the aggregation number decreases from 174 to 73 with decreasing molecular weight of the polymer.

The measured SAXS curves were used to calculate the PDDF via IFT and by deconvolution of the PDDF the radial contrast profile $\Delta\rho(r)$ was obtained. In Figure 7, the PDDF and the corresponding fits from the deconvolution of series B are shown. As expected the maximum size of the micelles decreases with decreasing molecular weight of the polymers **5**, **10**−**13** and is in good agreement with the maxima obtained by DLS. The shape of the PDDF does not change much; that implies that the micellar structure is also basically the same for the five different block copolymers, but scaled in size for the whole series. From the relatively symmetrical shape of the PDDF one can assume spherical geometry of the micelles. In Figure 8, the radial contrast profiles from the deconvolution using spherical symmetry are shown. Spline functions were used to build up the contrast profile. To take different particle number densities into

Table 3. Micellar Dimensions from Deconvolution Using a Two Step Model and Calculated Shell Sizes (R_E) of the Lyophilic Part (Self-Avoiding Walk Model)

	sample no.	radius of core, nm	thickness of the shell, nm	end-to-end distance of the lyophilic part, nm
series A	3	14.0	10.0	8.8
	4	12.0	12.0	11.1
	5	11.5	15.5	13.2
	6	9.5	15	15.1
	7	5.5	15.5	16.8
	8			
series B	5	11.5	15.5	13.2
	10	9.5	11.5	11.1
	11	7.0	8.0	7.7
	12	6.0	6.5	6.5
	13	4.5	5.5	5.1

Scheme 2. Schematic Presentation of the Radial Contrast Profile of the Series B Polymers 5, 10−13 Where L_c is the Radius of the Core and L_s is the Thickness of the Shell[a]

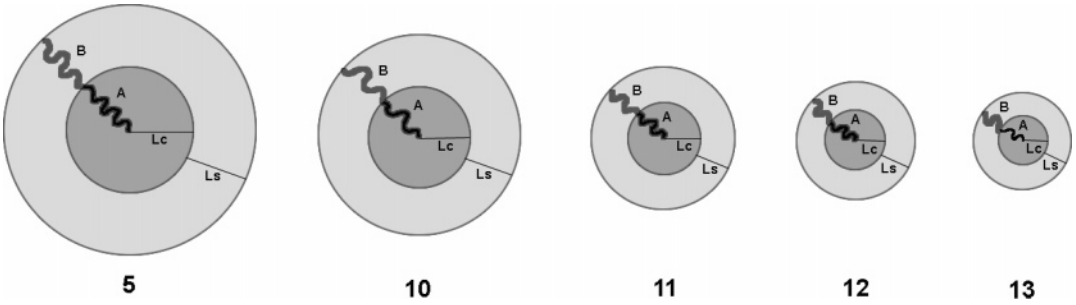

[a] The values for L_c and L_s determined by the two step model are listed in Table 3.

Scheme 3. Schematic Presentation of the Radial Contrast Profiles of the Series A Polymers 3−7 Where L_c is the Radius of the Core and L_s is the Thickness of the Shell[a]

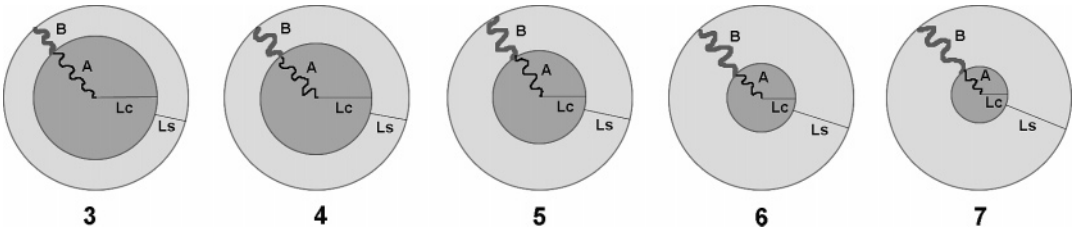

[a] The values for L_c and L_s determined by the two step model are listed in Table 3.

account the contrast profiles were multiplied by the square root of the area under the corresponding PDDF, which is proportional to the particle volume. All of the contrast profiles show a core−shell structure with a relatively high contrast of the core to the shell. The electron densities of both blocks of the polymer are in principle almost the same. The contrast from the lyophobic core to the lyophilic shell is however relatively large as the core consists mainly of lyophobic chains whereas in the lyophilic shell a lot of solvent is incorporated. This means the electron density of the shell is much closer to that of the solvent. The contrast of the micellar core to the shell is about the same for all polymers of this series if one considers the size of the error bars. As a result of the core−shell structure of the micelles, the deconvolution of the PDDF was repeated using a two step model. Four parameters were varied: the radii of the core and the shell and the electron density in both steps. The micellar dimensions determined by this method are shown in Table 3. The radial contrast profile from Figure 8 and Table 3 is graphically depicted in Scheme 2. It is shown that the size of the core is for all polymers of this series approximately half of the size of the whole micelle. The radius which was measured with DLS is somewhat smaller than the maximum dimension of the contrast profile but larger than the core size, which is reasonable because the micelles might not behave like hard spheres. The fits of the deconvolution processes are good, as can be seen in Figure 7. Only at the largest dimension, where one reaches the resolution limit the fit does deviate significantly.

In Figures 9 and 10, the equivalent data for the series A poylmers **3**−**8** is shown. In this series the size of the micelles is basically unchanged, except for **8**, which was the most lyophilic, where it was not possible to calculate a reasonable PDDF. However the shape of the PDDFs changes significantly. The PDDF of polymer **3** with the largest lyophobic block looks almost like a PDDF of a homogeneous sphere. The smaller the lyophobic block is the broader the peak of the PDDF becomes. Additionally the area below the curve becomes smaller, which means that the contrast in electron density is decreasing. This can be easily explained with reference to the composition of

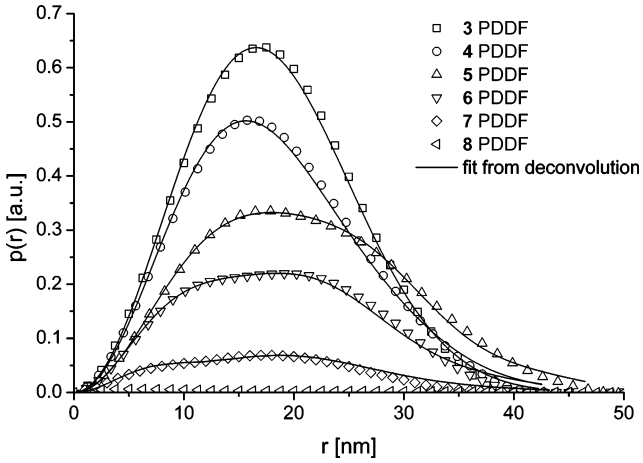

Figure 9. Pair distance distribution functions $p(r)$ (symbols) of polymers **3**−**8** (series A) having varying lyophobic-to-lyophilic ratio X_m determined via IFT from SAXS curves. The ratio X_m is decreasing from **3** (3.2) to **8** (0.14). The lines are the corresponding fits from the deconvolution.

the block copolymers. The lyophilic shell of **3** is thin; the micelles look more or less like homogeneous spheres. The thicker the shell gets the more solvent is incorporated into the micelles and the more visible the inhomogeneity becomes. This causes the decreasing overall contrast, and is also in agreement with the finding that the molecular weight of the micelles (Table 2) decreases (decreasing aggregation number) and the micellar size stays essentially the same.

These conclusions are also consistent with the radial contrast profiles (Figure 10) and the micellar dimensions (Table 3). The size of the core decreases with decreasing X_m, and the thickness of the shell increases at the same time. The diameter of the all the micelles is almost constant. The results are also schematically depicted in Scheme 3. Again the size determined by DLS is somewhat smaller than the maximum size of the contrast profile but larger than the core size.

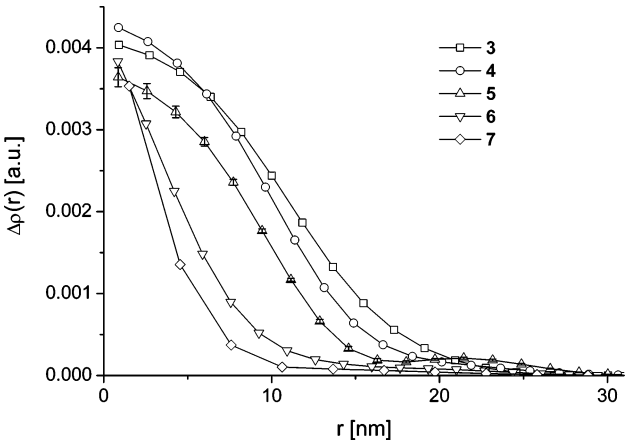

Figure 10. Radial contrast profile $\Delta\rho(r)$ of polymers **3**−**7** (series A) having varying lyophobic-to-lyophilic ratio X_m determined via deconvolution from the PDDF. The ratio X_m is decreasing from **3** (3.2) to **7** (0.31).

For an estimation of core and shell dimensions, the radius of gyration of polymer **9** (200 units of the lyophilic monomer) was determined to be 8.1 nm leading to a value for the constant *c* of eq 7 of about 0.36 nm. This allows us the estimation of end-to-end distances R_E of the lyophilic blocks which are listed in Table 3. The good agreement of the measured shell thickness and the calculated values for the end-to-end distance show that the thickness of the shell scales with the number of lyophilic units as expected for a self-avoiding walk model. As there was no R_g accessible for the pure lyophobic polymer, because it is not soluble in ethanol, such a calculation was restricted to the lyophilic moieties.

Comparing both series, all polymers which were soluble in ethanol form stable spherical micelles. In Table 3 it is shown that the micelle size as well as the core and shell size can be tuned on the nanometer range via the composition of the block copolymer. For series A the radius of the micelles stays about the same while the radius of the core is decreasing and in series B the ratio of core to shell radius is for all block copolymers about 1:1.

Conclusion

Block copolymers derived from ROMP are becoming more and more interesting for many applications. In this contribution we presented the synthesis of well-defined amphiphilic block copolymers via ROMP and the investigation of their self-assembly in solution. We introduced the *tert*-butyl group as protection group for the acidic functionalities to enable controlled synthesis and complete characterization of the precursor block copolymer. After cleavage of the protection group, amphiphilic block copolymers were obtained. We investigated their micelle formation in ethanol on two exemplary series: in series A the ratio of the lyophilic to the lyophobic block was altered but the overall polymer length was retained. In series B the ratio was fixed to 1:1 but the polymer length was varied. In series A, all polymers formed stable micelles in ethanol, apart from polymer **2** with the highest lyophobic fraction, which was insoluble, and polymer **8** with the highest lyophilic fraction which was completely dissolved in ethanol. For this series the overall micelles size stays about the same while the core size decreases linearly with increasing lyophilic fraction. In series B, the micelle size decreases linearly with decreasing polymer size. The core-to-shell ratio behaves like the block ratio and is constant for this series. To summarize these results, we have shown that it is possible to design well-defined amphiphilic block copolymers by the "*tert*-butyl route". It is possible to tune precisely the micelle size as well as the core and shell size on the nanometer range via the composition of the block copolymer.

Acknowledgment. The authors thank the Austrian Science Fund in the framework of the Austrian Nano Initiative (RPC0700-RP0701 and RP 0705) for financial support, Christian Slugovc for helpful discussion, Petra Kaschnitz for the NMR measurements and Josefine Hobisch for the GPC measurements, and the project students Marsha Loth and Christoph Auner.

References and Notes

(1) Lodge, T. P. *Macromol. Chem. Phys.* **2003**, *204*, 265−273.
(2) Forster, S.; Plantenberg, T. *Angew. Chem., Int. Ed.* **2002**, *41*, 689−714.
(3) Hamley, I. W.; Castelletto, V. *Prog. Polym. Sci.* **2004**, *29*, 909−948.
(4) Gohy, J.-F. *Adv. Polym. Sci.* **2005**, *190*, 65−136.
(5) Rodriguez-Hernandez, J.; Checot, F.; Gnanou, Y.; Lecommandoux, S. *Prog. Polym. Sci.* **2005**, *30*, 691−724.
(6) Baradie, B.; Shoichet, M. S. *Macromolecules* **2002**, *35*, 3569−3575.
(7) Lele, B. S.; Leroux, J. C. *Macromolecules* **2002**, *35*, 6714−6723.
(8) Gref, R.; Minamitake, Y.; Peracchia, M. T.; Trubetskoy, V.; Torchilin, V.; Langer, R. *Science* **1994**, *263*, 1600−1603.
(9) Kataoka, K.; Harada, A.; Nagasaki, Y. *Adv. Drug Delivery Rev.* **2001**, *47*, 113−131.
(10) Kane, R. S.; Cohen, R. E.; Silbey, R. *Chem. Mater.* **1996**, *8*, 1919−1924.
(11) Liaw, D. J.; Huang, C. C.; Wu, P. L. *Polymer* **2001**, *42*, 9371−9377.
(12) Liaw, D. J.; Wu, P. L. *J. Mol. Catal. A: Chem.* **2000**, *160*, 35−43.
(13) Clay, R. T.; Cohen, R. E. *Supramol. Sci.* **1997**, *4*, 113−119.
(14) Emoto, K.; Nagasaki, Y.; Kataoka, K. *Langmuir* **1999**, *15*, 5212−5218.
(15) Liu, J. Q.; Zhang, Q.; Remsen, E. E.; Wooley, K. L. *Biomacromolecules* **2001**, *2*, 362−368.
(16) Lynn, D. M.; Kanaoka, S.; Grubbs, R. H. *J. Am. Chem. Soc.* **1996**, *118*, 784−790.
(17) Nguyen, S. T.; Johnson, L. K.; Grubbs, R. H.; Ziller, J. W. *J. Am. Chem. Soc.* **1992**, *114*, 3974−3975.
(18) Oskam, J. H.; Schrock, R. R. *J. Am. Chem. Soc.* **1993**, *115*, 11831−11845.
(19) Schrock, R. R. *Acc. Chem. Res.* **1990**, *23*, 158−165.
(20) Harries-Rees, K.; Chauvin, Y.; Grubbs, R.; Schrock, R. *Chem. World* **2005**, *2*, 42−44.
(21) Riegler, S.; Slugovc, C.; Trimmel, G.; Stelzer, F. *Macromol. Symp.* **2004**, *217*, 231−246.
(22) Buchmeiser, M. R. *Chem. Rev.* **2000**, *100*, 1565−1604.
(23) Carrillo, A.; Kane, R. S. *J. Polym. Sci., Part A: Polym. Chem.* **2004**, *42*, 3352−3359.
(24) Dalphond, J.; Bazzi, H. S.; Kahrim, K.; Sleiman, H. F. *Macromol. Chem. Phys.* **2002**, *203*, 1988−1994.
(25) Ahmed, S. R.; Bullock, S. E.; Cresce, A. V.; Kofinas, P. *Polymer* **2003**, *44*, 4943−4948.
(26) Chemtob, A.; Heroguez, V.; Gnanou, Y. *Macromolecules* **2004**, *37*, 7619−7627.
(27) Liaw, D. J.; Chen, T. P.; Huang, C. C. *Macromolecules* **2005**, *38*, 3533−3538.
(28) Bertin, P. A.; Smith, D. D.; Nguyen, S. T. *Chem. Commun.* **2005**, 3793−3795.
(29) Bertin, P. A.; Watson, K. J.; Nguyen, S. T. *Macromolecules* **2004**, *37*, 8364−8372.
(30) Chen, B. Z.; Sleiman, H. F. *Macromolecules* **2004**, *37*, 5866−5872.
(31) Bazzi, H. S.; Sleiman, H. F. *Macromolecules* **2002**, *35*, 624−629.
(32) Gratt, J.; Cohen, R. E. *Macromolecules* **1997**, *30*, 3137−3140.
(33) Royappa, A. T.; Saunders, R. S.; Rubner, M. F.; Cohen, R. E. *Langmuir* **1998**, *14*, 6207−6214.
(34) Ahmed, S. R.; Kofinas, P. *Macromolecules* **2002**, *35*, 3338−3341.
(35) Clay, R. T.; Cohen, R. E. *Supramol. Sci.* **1998**, *5*, 41−48.
(36) Clay, R. T.; Cohen, R. E. *New J. Chem.* **1998**, *22*, 745−748.
(37) Slugovc, C.; Demel, S.; Riegler, S.; Hobisch, J.; Stelzer, F. *J. Mol. Catal. A: Chem.* **2004**, *213*, 107−113.
(38) Slugovc, C. *Macromol. Rapid Commun.* **2004**, *25*, 1283−1297.
(39) Slugovc, C.; Demel, S.; Riegler, S.; Hobisch, J.; Stelzer, F. *Macromol. Rapid Commun.* **2004**, *25*, 475−480.
(40) Ahmed, S. R.; Ogale, S. B.; Papaefthymiou, G. C.; Ramesh, R.; Kofinas, P. *Appl. Phys. Lett.* **2002**, *80*, 1616−1618.
(41) Saunders, R. S.; Cohen, R. E.; Wong, S. J.; Schrock, R. R. *Macromolecules* **1992**, *25*, 2055−2057.

(42) Kanaoka, S.; Grubbs, R. H. *Macromolecules* **1995**, *28*, 4707−4713.
(43) Buchmeiser, M. R.; Atzl, N.; Bonn, G. K. *J. Am. Chem. Soc.* **1997**, *119*, 9166−9174.
(44) Koch, H.; Kotlan, J.; Markut, H. *Monatsh. Chem.* **1965**, *96*, 1646−1657.
(45) Schnablegger, H.; Glatter, O. *Appl. Opt.* **1991**, *30*, 4889−4896.
(46) Crivello, J. V.; Shim, S. Y. *Chem. Mater.* **1996**, *8*, 376−381.
(47) Chu, B. *Laser Light Scattering*, 2nd ed.; Academic Press: San Diego, CA, 1991.
(48) Berne, B. J.; Pecora, R. *Dynamic Light Scattering*; John Wiley & Sons: New York, 1976.
(49) Pecora, R., Ed. *Dynamic Light Scattering*; Plenum Press: New York, 1985.
(50) Brown, W., Ed. *Dynamic Light Scattering: The Method and Some Applications*; Clarendon Press: Oxford, U.K., 1993.
(51) Einstein, A. *Annal. Phys. (Weinheim, Germany)* **1905**, *17*, 549−560.
(52) Provencher, S. W. *Comput. Phys. Commun.* **1982**, *27*, 213−227.
(53) Jakes, J. *Collect. Czechoslovak Chem. Commun.* **1995**, *60*, 1781−1797.
(54) Fritz, G.; Scherf, G.; Glatter, O. *J. Phys. Chem. B* **2000**, *104*, 3463−3470.
(55) Orthaber, D.; Bergmann, A.; Glatter, O. *J. Appl. Crystallogr.* **2000**, *33*, 218−225.
(56) Glatter, O. *J. Appl. Crystallogr.* **1977**, *10*, 415−421.
(57) Glatter, O. *J. Appl. Crystallogr.* **1980**, *13*, 577−584.
(58) Glatter, O., Kratky, O., Eds. *Small-angle X-ray scattering*; Academic Press: London, 1982.
(59) Brunner-Popela, J.; Glatter, O. *J. Appl. Crystallogr.* **1997**, *30*, 431.
(60) Weyerich, B.; Brunner-Popela, J.; Glatter, O. *J. Appl. Crystallogr.* **1999**, *32*, 197−209.
(61) Bergmann, A.; Fritz, G.; Glatter, O. *J. Appl. Crystallogr.* **2000**, *33*, 1212−1216.
(62) Kratky, O.; Porod, G.; Kahovec, L. *Z. Elektrochem. Angew. Phys. Chem.* **1951**, *55*, 53−59.
(63) Glatter, O. *J. Appl. Crystallogr.* **1981**, *14*, 101.
(64) Glatter, O.; Hainisch, B. *J. Appl. Crystallogr.* **1984**, *17*, 435−441.
(65) Mittelbach, R.; Glatter, O. *J. Appl. Crystallogr.* **1998**, *31*, 600−608.
(66) Evans, D. F.; Wennerström, H. *The Colloidal Domain*; VCH: New York, 1994; Chapter 4.

MA060451P